

Enhanced multiscale quantum approximate optimization algorithm in multibody combinatorial optimization problems

Lei-Lei Chen(陈蕾蕾), Ping Zou(邹平), and Ya-Fei Yu(於亚飞)
Citation: Chin. Phys. B, 2026, 35 (**7**): 070305. DOI: 10.1088/1674-1056/ae29f7
http://cpb.iphy.ac.cn; http://iopscience.iop.org/cpb

What follows is a list of articles you may be interested in

Coherence and decoherence in generalized Shor's algorithm

Linlin Ye(叶琳琳), Zhaoqi Wu(吴照奇), and Nanrun Zhou(周南润)
Chin. Phys. B, 2026, 35 (**6**): 060304. DOI: 10.1088/1674-1056/ae445e

Auxiliary-qubit-free quantum approximate optimization algorithm for the minimum dominating set problem

Guanghui Li(李广辉), Xiaohui Ni(倪晓慧), Junjian Su(苏俊健), Sujuan Qin(秦素娟), Fenzhuo Guo(郭奋卓), Bingjie Xu(徐兵杰), Wei Huang(黄伟), and Fei Gao(高飞)
Chin. Phys. B, 2026, 35 (**5**): 050304. DOI: 10.1088/1674-1056/ae5052

Efficient fault-tolerant circuit for preparing quantum uniform superposition states via quantum measurement

Xiang-Qun Fu(付向群), Tian-Ci Tian(田天赐), Hong-Wei Li(李宏伟), Jian-Hong Shi(史建红), Xiao-Liang Yang(杨晓亮), Tan Li(李坦), and Wan-Su Bao(鲍皖苏)
Chin. Phys. B, 2025, 34 (**12**): 120303. DOI: 10.1088/1674-1056/addcc2

Progressive quantum algorithm for maximum independent set with quantum alternating operator ansatz

Xiao-Hui Ni(倪晓慧), Ling-Xiao Li(李凌霄), Yan-Qi Song(宋燕琪), Zheng-Ping Jin(金正平), Su-Juan Qin(秦素娟), and Fei Gao(高飞)
Chin. Phys. B, 2025, 34 (**7**): 070304. DOI: 10.1088/1674-1056/addd83

Distributed quantum circuit partitioning and optimization based on combined spectral clustering and search tree strategies

Zilu Chen(陈子禄), Zhijin Guan(管致锦), Shuxian Zhao(赵书娴), and Xueyun Cheng(程学云)
Chin. Phys. B, 2025, 34 (**5**): 050305. DOI: 10.1088/1674-1056/adbada

---

Enhanced multiscale quantum approximate optimization algorithm in multibody combinatorial optimization problems

Lei-Lei Chen(陈蕾蕾)[1], Ping Zou(邹平)[1,†], and Ya-Fei Yu(於亚飞)[1,2,‡]

[1] *Guangdong Provincial Key Laboratory of Nanophotonic Functional Materials and Devices, School of Optoelectronic Science and Engineering, South China Normal University, Guangzhou* 510006, *China*

[2] *Quantum Science Center of Guangdong–Hong Kong–Macao Greater Bay Area, Shenzhen* 518109, *China*

(Received 17 July 2025; revised manuscript received 26 November 2025; accepted manuscript online 9 December 2025)

At present, the quantum approximate optimization algorithm (QAOA) faces scalability challenges in high-dimensional combinatorial optimization problems due to exponentially growing computational costs and reachability deficits for noisy intermediate-scale quantum (NISQ) devices. This study focuses on the multiscale quantum approximate optimization algorithm (MQAOA), which integrates renormalization group (RG) transformations with QAOA to address these limitations. Based on the connections between the variables in the problem to be solved, the weighted maximal matching method is employed to generate a variable partitioning strategy guiding the RG transformation. This approach not only extends the applicability of MQAOA to satisfiability (SAT) problems — including those with three-body and higher-order interactions in the problem Hamiltonian — but also eliminates the algorithm's sensitivity to problem density. Validations conducted on quantum simulators show that, after running two-round MQAOA, its capability is enhanced to identify optimal solutions with approximately 97% success probability as defined by the ground-state overlap for Max-2-SAT problems (78% success probability for Max-3-SAT problems). The results confirm the feasibility of MQAOA and establish it as a resource-efficient framework for complex combinatorial optimization problems, providing a pathway for NISQ-era deployment.

Keywords: quantum algorithm, parameterized quantum circuit, renormalization group transformation, combinatorial optimization, Max-SAT problems

PACS: 03.67.Ac, 03.67.Lx, 03.67.–a

DOI: 10.1088/1674-1056/ae29f7 **CSTR:** 32038.14.CPB.ae29f7

1. Introduction

The era of noisy intermediate-scale quantum (NISQ) devices has arrived, which has accelerated the development of quantum algorithms that demonstrate potential quantum advantage.[1] Among these, hybrid quantum-classical algorithms emerge as a promising strategy to mitigate quantum decoherence challenges while maintaining computational efficiency.[2,3] Notably, the quantum approximate optimization algorithm (QAOA)[4,5] has established itself as a versatile framework for combinatorial optimization, with successful applications spanning from traveling salesman problems[6,7] to molecular docking simulations.[8,9] By iteratively optimizing parameterized quantum circuits through classical methods, QAOA enables systematic convergence toward problem solutions.

Despite these advancements, critical limitations persist in implementing standard QAOA, which hinder its broader application: (1) reachability deficits in high clause density maximum satisfiability (Max-SAT) problems,[10–12] where algorithm performance degrades with increasing constraint complexity, and (2) excessive parameters, which make parameter optimization difficult and have a negative effect on the performance of the algorithm.[13] While recent improvements through Hamiltonian modifications[14–18] and parameter optimization strategies[19–21] have partially addressed these issues, reachability deficits remain.

Multiscale quantum approximate optimization algorithm (MQAOA) in Ref. [22] integrates renormalization group (RG) transformations into QAOA to overcome reachability deficits and suppress the number of parameters to be optimized. In Ref. [22], the applications of MQAOA are limited to problems including only two-body interactions in the problem Hamiltonian, such as the MaxCut problem, Max-2-SAT problem, and Ising spin glass models, which have an obvious and simple connection graph derived from their problem Hamiltonians so that each two adjacent qubits are matched and mapped to a single qubit through RG transformation. As the authors stated, the performance ratio depends on a specific partition scheme, and the efficiency of MQAOA with a depth-1 QAOA embedded decreases as the scale of the connection graph increases. Various maximal matchings are suggested to overcome these issues. Hence, in the present work, we propose an approach that extends MQAOA's application to cases where the problem Hamiltonian includes not only two-body interactions but also three-body and higher-order interactions. It searches for

†Corresponding author. E-mail: zouping@m.scnu.edu.cn

‡Corresponding author. E-mail: yuyafei@m.scnu.edu.cn

© 2026 Chinese Physical Society and IOP Publishing Ltd. All rights, including for text and data mining, AI training, and similar technologies, are reserved.

partition and maximal matching strategies through a weighted connection graph constructed according to the connections of variables in the problem. As a result, the enhanced MQAOA requires only one layer of standard QAOA quantum circuit to find the optimal solution for Max-SAT problems, even when including interactions involving more than two variables and higher-than-two-body interactions; meanwhile, an order-of-magnitude reduction in energy error is achieved. Under the same number of layers of standard QAOA, the performance of the enhanced MQAOA does not degrade with increasing clause density. We validate the enhanced MQAOA through quantum simulations for Max-2/3-SAT problems on the Origin Quantum Cloud Platform, showing maintained performance under increasing clause density. These results establish a foundation for solving broader classes of multi-body combinatorial optimization problems with MQAOA.

The remainder of this paper is organized as follows. Brief overviews of MQAOA based on standard QAOA and SAT problems are given in Section 2. In Section 3, an enhanced MQAOA is proposed for multiple SAT problems including two-body and three-body interactions, with its demonstration on the Origin Quantum Simulator in Section 4. The concluding remarks follow in Section 5.

2. The framework of multiscale quantum approximate optimization algorithm

The quantum approximate optimization algorithm (QAOA) is established for combinatorial optimization problems.[4,5] The core idea of QAOA is to construct parameterized quantum circuits by alternately applying the Hamiltonian H_C related to the problem to be solved and the mixing Hamiltonian H_B. Through combination with classical optimization algorithms, which adjust the parameters of the quantum circuit, the expectation value of the problem Hamiltonian is minimized step by step. The initial state of the quantum system is generally prepared as a uniform superposition of all possible solutions $|+\rangle^{\otimes n}$.

The mixing Hamiltonian is chosen as

$$H_B = \sum_{j=1}^{n} \sigma_j^x, \tag{1}$$

where σ_j^x denotes the Pauli X operator applied to the j-th qubit. The parameterized quantum circuit is constructed by alternately applying the problem Hamiltonian H_C and the mixing Hamiltonian H_B, and is expressed as

$$U(\beta,\gamma) = \prod_{k=1}^{P} \mathrm{e}^{-\mathrm{i}\beta_k H_B}\, \mathrm{e}^{-\mathrm{i}\gamma_k H_C}, \tag{2}$$

where P denotes the number of layers within the parameterized quantum circuit. All time-evolution parameters β_k and γ_k are randomly selected from the interval $[-\pi/2, \pi/2]$. The initial state $|+\rangle^{\otimes n}$ evolves into a parameterized ansatz state after the P-th layer of the parameterized quantum circuit

$$|\psi(\beta,\gamma)\rangle = \prod_{k=1}^{P} \mathrm{e}^{-\mathrm{i}\beta_k H_B}\, \mathrm{e}^{-\mathrm{i}\gamma_k H_C} |+\rangle^{\otimes n}. \tag{3}$$

The expectation value of the problem Hamiltonian H_C in the ansatz state is then measured as

$$\langle H_C \rangle = \langle \psi(\beta,\gamma) | H_C | \psi(\beta,\gamma) \rangle . \tag{4}$$

A lower expectation value indicates that the ansatz state is closer to the ground state of the problem Hamiltonian. Solving a combinatorial optimization problem is equivalent to finding an objective state $|z\rangle$ that minimizes the expectation value of the target Hamiltonian, i.e., $\min \langle H_C \rangle = \langle z|H_C|z\rangle$. However, the performance of QAOA is negatively impacted by an increase in the clause density of Max-SAT problems, a limitation known as reachability deficits. Although increasing the number of layers in the quantum circuit can alleviate this issue, it leads to a significant rise in computational complexity.

MQAOA was proposed to resolve this issue.[22] The key step in MQAOA lies in the use of the RG transformation to aid in finding the ansatz state in QAOA, a numerical method employed for system coarse-graining.[23] In quantum systems, the RG transformation focuses on the controllable compression of the Hilbert space dimension, thereby reducing its degrees of freedom. Specifically, for a quantum system defined on a graph L with multiple vertices S, its Hilbert space is represented as

$$V_L = \bigotimes_{S\in L} V_S. \tag{5}$$

The graph L is partitioned into blocks based on maximal matching M, which can be obtained from the connections in the graph L by a classical algorithm. For simplicity, two adjacent vertices S_i and S_j paired through maximal matching form a block B. The Hilbert space of block B is denoted as V_B

$$V_L = \bigotimes_{B\in L} V_B, \quad V_B = \bigotimes_{S\in B} V_S. \tag{6}$$

Subsequently, we truncate the Hilbert space dimension of block B, coarse-graining it into an effective single vertex S'. The coarse-graining process can be represented by the isometry ω, which denotes the mapping relationship between the spaces V_B and $V_{S'}$

$$\omega : V_{S'} \to V_B, \quad \omega\omega^\dagger = \Pi, \tag{7}$$

where Π denotes a projection operator. By coarse-graining all blocks B in graph L, a set of effective vertices S' is obtained, which form a new graph L' with a reduced number of vertices, where $S' \in L'$. The effective Hamiltonian $H_{C'}$ for the new graph L' is

$$H_{C'} = W^\dagger H_C W, \tag{8}$$

where W represents the mapping between the original graph L and the new graph L'. The mapping W can be expressed as a tensor product $W = \otimes\omega_k$, where ω_k denotes the isometry corresponding to the k-th block. Using this method, the original multi-vertex graph L is coarse-grained into a new graph L' with fewer vertices.

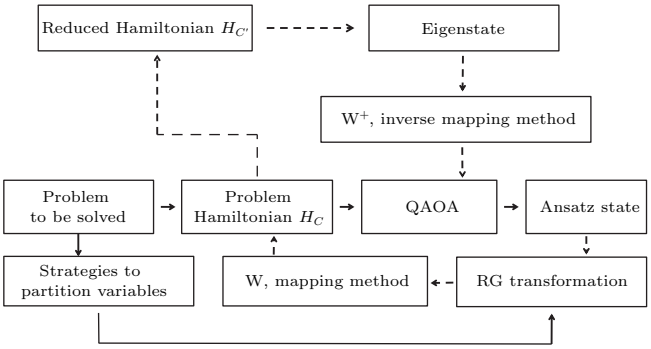


Fig. 1. Flow chart for MQAOA.

The specific procedure of MQAOA shown in Fig. 1 is explained as follows:

(i) Establishing a connection graph L characterized by the problem to be solved.

(ii) Searching for the maximal matching M of graph L through a classical algorithm.

(iii) Executing the first-layer QAOA circuit from the initial state $|+\rangle^{\otimes n}$ characterized by the problem Hamiltonian H_C and the mixing Hamiltonian H_B, yielding an ansatz state $|\psi(\beta,\gamma)\rangle$.

(iv) From the ansatz state, obtaining the reduced density matrix ρ_{ij} of each pair of the i-th and j-th qubits in blocks given in M.

(v) Performing the RG transformation on ρ_{ij} to derive a low-rank approximation matrix ρ_k of ρ_{ij}. This process condenses the main information in the block into an effective single qubit. A new coarse-grained graph L' of all effective qubits is constructed for the ansatz state. Finally, the isometry mapping W is established.

(vi) Creating the effective Hamiltonian $H_{C'}$ of the graph L' by applying W to the problem Hamiltonian H_C, denoted as $H_C' = W^\dagger H_C W$.

(vii) Finding the ground state $|\varphi_0{}'\rangle$ of the effective Hamiltonian $H_{C'}$, and preparing a new initial state $|\varphi\rangle = W|\varphi_0{}'\rangle$ as the initial testing state for QAOA in the next round of MQAOA. The first-round MQAOA with a depth-1 QAOA embedded is completed.

Repeat steps (iii)–(vii) until the expectation value of the target Hamiltonian converges. In step (ii), a highly efficient classical algorithm for maximum matching is required for graph preprocessing. It is important to note that a maximal matching is typically not unique, and different matching schemes can be utilized to improve the efficiency of MQAOA when the scale of the problem increases or the problem Hamiltonian becomes more complicated. The problem Hamiltonian in all application examples of MQAOA given in Ref. [22] involves only two-body interactions, which makes the edges in the graph L uniform and equally treated during matching. However, when the problem involves many variables, the Hamiltonian will inevitably consist of two-body interactions, three-body interactions, and higher-order interactions, which leads to the edges in the graph not being equally weighted, as mentioned in Ref. [24]. In the following, we take this issue into account and introduce edge weights into the maximal matching to extend the applicability of MQAOA.

3. Enhance MQAOA for multibody combinatorial optimization problems

Multibody combinatorial optimization problems are defined as optimization tasks involving interactions among multiple variables. In this section, we take the SAT problem as a representative example. The goal of the SAT problem is to find a set of Boolean variable assignments that satisfies a given Boolean formula, i.e., renders it true. A Boolean formula comprises two core components: Boolean variables and clauses. Each Boolean variable can take one of two values: TRUE or FALSE. In a Boolean formula, a Boolean variable (x_i) or its negation ($\neg x_i$) is called a literal (L_i). Literals are combined via the logical OR operation ($\vee$) to form clauses. An SAT instance is composed of m clauses linked by logical AND operations ($\wedge$). If each clause contains exactly k variables, the problem is termed a k-SAT problem. Its goal is to find a variable assignment that satisfies all clauses simultaneously.

3.1. Weighted connection graph of Max-SAT problems

Before performing the RG transformation, the maximal matching strategy M is obtained via a classical algorithm from the initial graph of the problem. Specifically, when applying MQAOA to the maximal Boolean satisfiability (Max-SAT) problem, we first construct a variable-connection graph according to the problem's structure. In general, there may be multiple connections between the same pair of variables, which complicates inter-variable relationships. To more precisely capture this complexity, we establish a weighted connection graph to reflect the strength of connections between variables.

We take the Max-3-SAT problem as an example to explain how to establish a weighted connection graph for the problem. Two instances of the Max-3-SAT problem with four variables can be expressed as

$$\begin{aligned} \Phi_1 &= (x_1 \vee x_2 \vee x_4), \\ \Phi_2 &= (x_1 \vee x_2 \vee x_3) \wedge (x_1 \vee x_2 \vee x_4). \end{aligned} \tag{9}$$

As illustrated in Fig. 2, we map Boolean variables to vertices in the graph and draw edges between vertices based on each clause. The variable connections in problem Φ_1 are shown in Fig. 2(a), while those in problem Φ_2 are shown in Fig. 2(b). It can be found that the connection between variables 1 and 2 occurs twice in problem Φ_2, so the edge between vertices 1 and 2 is assigned a weight of 2. Thus, the key aspect of establishing a weighted connection graph is to count the number of occurrences of connections between variable pairs, regardless of the sign of Boolean variables.

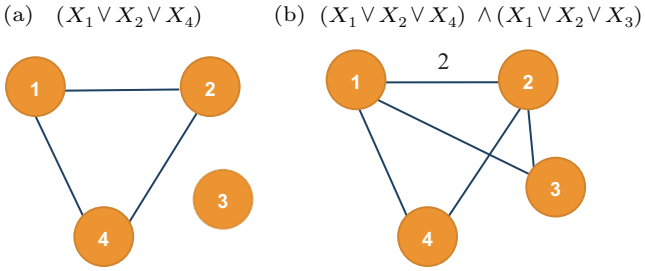


Fig. 2. The weighted connection graph of Max-3-SAT problem.

However, the weights of connecting edges cannot be explicitly reflected in the problem Hamiltonian, because Boolean variables are expressed as linear combinations of unitary operators. The Max-3-SAT problem can be encoded into the following Hamiltonian:

$$H_C = \sum_{r=1}^{m} (L_i \otimes L_j \otimes L_k)_r$$
$$= \frac{1}{8}\left(mI + \sum_i h_i \sigma_z^i + \sum_{i<j} f_{ij}\sigma_z^i\sigma_z^j + \sum_{i<j<k} g_{ijk}\sigma_z^i\sigma_z^j\sigma_z^k\right), \quad (10)$$

where m is the total number of clauses, and r denotes the clause index. L_i represents the i-th literal, which is expressed as a linear combination of the unitary operators I and σ_z:

$$L_i = \frac{1}{2}(I \pm \sigma_z^i). \quad (11)$$

For the problem Φ_2, the coefficients in the Hamiltonian are listed in Table 1. The coefficients of the unmentioned terms are zero. The coexistence of two-body and three-body interactions in the problem Hamiltonian makes it difficult to directly construct a connection graph. Instead, we use a weighted connection graph — constructed based on inter-variable relationships in the problem — to identify the optimal strategy for partitioning variables into blocks and performing RG transformations. It is important to note that one identical weighted connection graph may correspond to multiple different Hamiltonians, and vice versa. Once a problem is specified, the weighted connection graph must first be defined. This graph then serves as a guide for both the variable partitioning step and the subsequent RG transformations throughout the MQAOA process.

The weighted matching method based on weighted connection graphs needs to satisfy the following constraints: the principle of no repeated vertex matching and the global weight maximization criterion. That is, among all possible matches, the combination of two adjacent vertices with higher edge weight is preferred, ensuring that the sum of the matched edge weights reaches its maximum value. We can use the `max weight matching` function in the NetworkX library in Python to generate the maximal weighted matching M. The complexity of max weight matching is $O(n^3)$.

Table 1. Coefficient for each item in the problem Hamiltonian of the Max-3-SAT problem Φ_2.

h_1	h_2	h_3	h_4	f_{12}	f_{13}	f_{23}	f_{14}	f_{24}	g_{123}	g_{124}
2	2	1	1	2	1	1	1	1	1	1

In the matching scheme we proposed, we aim to prioritize the coarse-graining of variable (qubit) pairs that appear more frequently in the clauses. This reduces the number of three-body interactions and higher-order interactions in the effective Hamiltonian, thereby facilitating the use of quantum algorithms to find its ground state.

3.2. Comparison between weighted and unweighted matchings

To further explore the specific impact of different matching schemes on algorithm performance, we select a Max-3-SAT problem with 12 bits and 100 clauses as the test case. We design two control groups for comparative simulations. The first group adopts the unweighted matching method, i.e., a standard maximal matching function, whose aim is to combine as many variables as possible. The second group employs a weighted maximal matching method, which takes into account the weights of edges between variables. Both methods are used to generate 30 distinct matching schemes M, respectively. For each method, we execute 6 rounds of MQAOA, with the energy error E adopted as the performance metric. The energy error is defined as

$$E = \min \langle\varphi| H_C |\varphi\rangle - E_0, \quad (12)$$

where $|\varphi\rangle$ is the quantum state finally prepared by MQAOA, $\langle\varphi| H_C |\varphi\rangle$ is the expectation value of the problem Hamiltonian in $|\varphi\rangle$, and E_0 is the exact ground-state energy of the problem Hamiltonian. The test results are shown in Fig. 3.

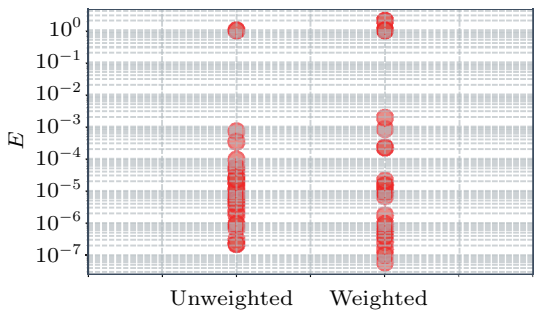


Fig. 3. Energy errors of MQAOA showing a Max-3-SAT problem with 12 bits and 100 clauses under unweighted and weighted matching methods.

In the unweighted matching scheme, the energy errors are mainly distributed at the order of magnitude of 10^{-5}, and the minimum energy error value is 2.19554×10^{-7}. In the weighted matching scheme, the energy errors are primarily concentrated at the order of magnitude of 10^{-6}, and the minimum energy error value is 5.95029×10^{-8}. The optimal result's energy error under the weighted matching scheme decreases by approximately 73% compared to the unweighted matching scheme, illustrating the significance of the edge weight parameter in the maximal matching process. Moreover, there are significant differences in energy errors under different matching schemes. In about 15% of the samples, a sharp increase in energy error occurs ($E \geq 1$), which may have a negative impact on algorithm performance. Therefore, in the coarse-graining process, a multi-path search mechanism should be adopted. This mechanism involves repeatedly computing k ($k \geq 5$) candidate matching schemes, comparing them, and selecting the one with the smallest energy error, thereby ensuring solution accuracy. Adopting this strategy can effectively overcome the problem of being trapped in local minima and further enhance solution quality.

3.3. Enhanced MQAOA vs. standard QAOA

In this section, we compare the performance of enhanced MQAOA and standard QAOA in solving the Max-SAT problem, revealing significant differences in the convergence speed of energy errors and the consumption of quantum resources.

We first compare the performance of standard QAOA and enhanced MQAOA in solving 30 Max-3-SAT instances with 12 variables and 100 clauses. In each round of the enhanced MQAOA, two energy error values are obtained: the first corresponds to the energy error of the ansatz state generated by depth-1 standard QAOA within that round, and the second corresponds to the energy error of the new initial state generated after RG transformation. The simulation results are presented in Fig. 4(a). Numerically, we observe that the energy error of the enhanced MQAOA approaches zero after only four rounds of iterative optimization. Each application of the RG transformation significantly reduces the energy error. In contrast, even when the number of layers increases to 6, the energy error of standard QAOA remains greater than 1 (see Fig. 4(b)); furthermore, the rate of decrease in energy error gradually slows as the number of layers in standard QAOA increases. Additionally, we examine the performance of these two algorithms on 30 Max-4-SAT problems with 12 variables and 100 clauses. Notably, enhanced MQAOA still computes an approximately optimal solution by the fourth round, while standard QAOA fails to solve the problem within 6 layers, as shown in Figs. 4(c) and 4(d).

To explore the universality of enhanced MQAOA, we extend its application to another variant of the SAT problem, namely the NAE3SAT problem.[25] It seeks to find a set of Boolean variable assignments such that the variables in the same clause are not all equal. Its corresponding Hamiltonian is given by

$$\hat{H}_C = \sum_{[i,j,k]\in C} [(s_i + s_j + s_k)^2 - 1]/2. \tag{13}$$

We randomly selected 20 instances of NAE-3-SAT problems, each with 10 variables and 100 clauses, solved them using both enhanced MQAOA and standard QAOA, and observed the variation in their energy errors as shown in Figs. 4(e) and 4(f). The observed results indicate that when solving the NAE-3-SAT problem, both algorithms exhibit relatively large variance in energy errors, with performance being less stable than when tackling the Max-SAT problem. Nevertheless, even under these conditions, enhanced MQAOA can still attain the optimal solution by the fourth round. In contrast, while standard QAOA shows improved performance at the sixth layer, it still lags behind enhanced MQAOA in optimization effectiveness.

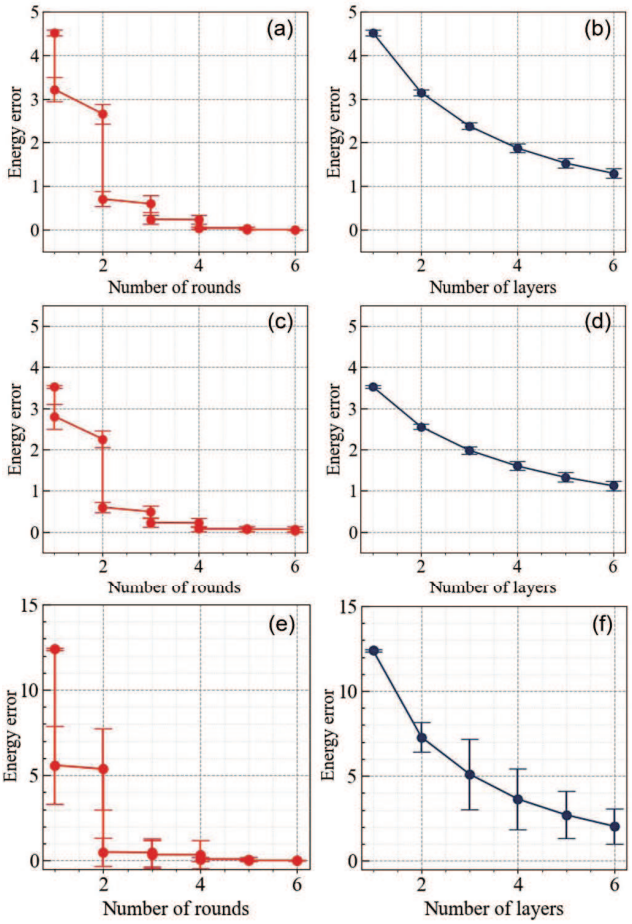


Fig. 4. Energy errors of enhanced MQAOA and standard QAOA for SAT problems. The data points represent the mean values of the data sets, and the error bars indicate the corresponding variations. (a) Enhanced MQAOA for Max-3-SAT. (b) QAOA for Max-3-SAT. (c) Enhanced MQAOA for Max-4-SAT. (d) QAOA for Max-4-SAT. (e) Enhanced MQAOA for NAE3SAT. (f) QAOA for NAE3SAT.

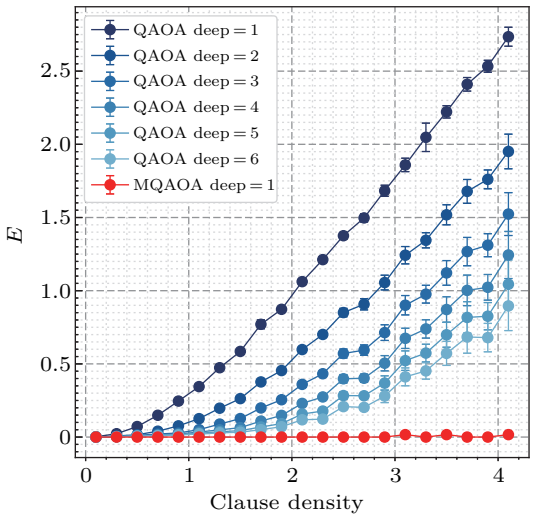


Fig. 5. Solving 60 Max-3-SAT problems with different clause densities by enhanced MQAOA with a single-layer quantum circuit (red) and standard QAOA with 1–6 layer quantum circuits (blue). The horizontal axis shows clause density and the vertical axis shows the energy error E. The error bars represent the variance of the data sets.

The comparison indicates that via RG transformation guided by weighted maximal matching, enhanced MQAOA can efficiently approximate the optimal solution within fewer rounds. In contrast, when handling complex optimization problems, standard QAOA may require more layers and a more complex quantum circuit architecture, and its energy error convergence rate is significantly slower than that of enhanced MQAOA.

We further explore the impact of clause density on the performance of enhanced MQAOA. To this end, we solve Max-3-SAT problems with 10 variables and a variable number of clauses ranging from 1 to 41. From Fig. 5, we observe that the energy error E in standard QAOA increases progressively as the clause density increases. By contrast, for enhanced MQAOA, the energy error does not increase with increasing clause density and consistently attains an approximately optimal solution. This demonstrates that enhanced MQAOA effectively mitigates the reachability deficits present in standard QAOA. Compared with standard QAOA, enhanced MQAOA offers clear advantages in solving multibody combinatorial optimization problems with high clause density.

4. The validation of enhanced MQAOA on the origin quantum simulator

In order to explore the possibility of running enhanced MQAOA on a real quantum computer, we validate the enhanced MQAOA on the Origin quantum simulator using Max-2-SAT and Max-3-SAT problems as examples, comparing it with standard QAOA in terms of computational efficiency and quantum resource cost. The algorithmic performance can be assessed using metrics such as energy error in the approximation and ground-state overlap, while the quantum computing cost can be measured by the number of gates required to implement the algorithm.

4.1. Solving Max-2-SAT problem by enhanced MQAOA

The Boolean formula for an instance of the Max-2-SAT problem with 5 bits and 15 clauses is given as

$$\begin{aligned}\Phi = &(\neg x_0 \vee x_1) \wedge (\neg x_0 \vee \neg x_2) \wedge (\neg x_0 \vee \neg x_3) \wedge (x_0 \vee \neg x_1) \\ &\wedge (x_0 \vee x_2) \wedge (\neg x_1 \vee \neg x_2) \wedge (\neg x_1 \vee x_2) \wedge (\neg x_1 \vee \neg x_3) \\ &\wedge (x_1 \vee x_3) \wedge (\neg x_3 \vee x_2) \wedge (x_3 \vee \neg x_2) \wedge (x_3 \vee x_2) \\ &\wedge (\neg x_4 \vee \neg x_2) \wedge (\neg x_4 \vee \neg x_3) \wedge (x_4 \vee x_3). \end{aligned} \tag{14}$$

The weighted connection graph for this instance is presented in Fig. 6. The corresponding weighted maximal matching for the graph is given by $M = [(0,1),(2,3)]$, with the sum of the weights of the matched edges attaining a maximal value of 5.

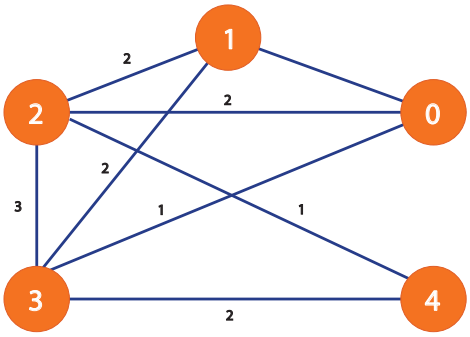


Fig. 6. The weighted connection graph for the instance of Max-2-SAT problem.

The coefficients of the terms in the problem Hamiltonian H_C related to Eq. (14) are presented in Table 2, with the coefficients of the unmentioned terms being zero.

Table 2. Coefficient for each item of H_C of Max-2-SAT problem.

h_0	h_1	h_4	f_{01}	f_{02}	f_{03}	f_{13}	f_{23}	f_{24}	f_{34}
−1	−2	−1	−2	2	1	2	-1	1	2

The evolution of the terms in the problem Hamiltonian H_C can be decomposed into a combination of quantum logic gates

$$\begin{aligned} &\mathrm{e}^{-\mathrm{i}\frac{\gamma h_i}{4}\sigma_z^i} = RZ(i, \frac{\gamma h_i}{2}), \\ &\mathrm{e}^{-\mathrm{i}\frac{\gamma f_{ij}}{4}\sigma_z^i \otimes \sigma_z^j} = \mathrm{CNOT}(i,j) \cdot RZ\left(j, \frac{\gamma f_{ij}}{2}\right) \cdot \mathrm{CNOT}(i,j). \end{aligned} \tag{15}$$

The evolution of the mixing Hamiltonian can be implemented using RX gates

$$\mathrm{e}^{-\mathrm{i}\sum_{j=1}^{n}\beta\sigma_x^j} = \prod_{j=1}^{n} \mathrm{e}^{-\mathrm{i}\beta\sigma_x^j} = \prod_{j=1}^{n} R_x(j, 2\beta). \tag{16}$$

The quantum circuit used to solve the instance of the Max-2-SAT problem in Eq. (15) with round-1 MQAOA is illustrated in Fig. 7.

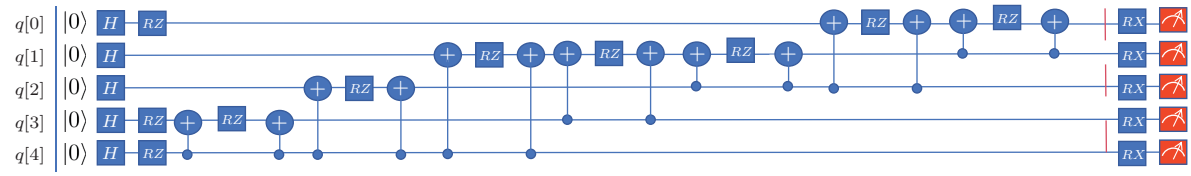


Fig. 7. Quantum circuit of depth-1 QAOA embedded in round-1 MQAOA for solving the Max-2-SAT instance, with qubits ordered in reverse relative to the variables in Eq. (15). The time parameters $(\gamma,\beta) = (0.73717232, -0.46441724)$.

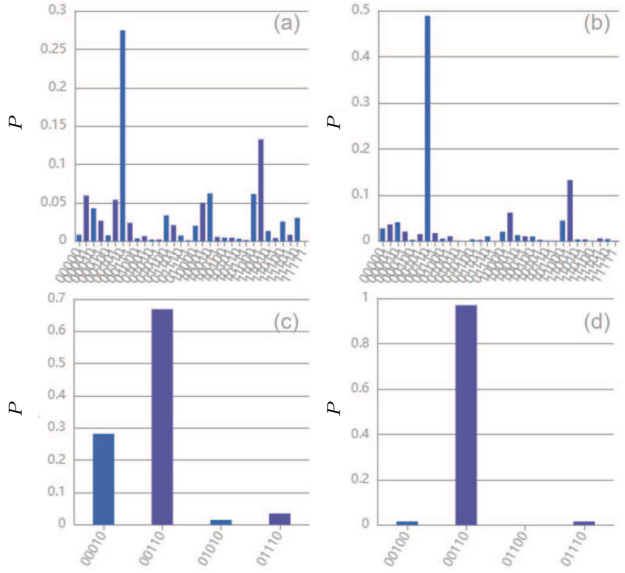


Fig. 8. The probability distribution of the output quantum state from QAOA and MQAOA for solving the Max-2-SAT problem. (a) depth-1 QAOA; (b) depth-2 QAOA; (c) round-1 MQAOA; (d) round-2 MQAOA.

After performing the RG transformation in round-1 MQAOA, the probability distribution of the prepared quantum state is shown in Fig. 8(c), which serves as the initial state of QAOA in round-2 MQAOA. The differences in the quantum circuit are shown in Fig. 9. The output quantum state of round-2 MQAOA is shown in Fig. 8(d).

For comparison, the solution of the Max-2-SAT instance is validated by depth-1 and depth-2 QAOAs. The quantum circuit for depth-1 QAOA is identical to that shown in Fig. 7, while the quantum circuit for depth-2 QAOA simply repeats the main part in Fig. 7, except for the initialization gates H, with time parameters $(\gamma_1,\beta_1,\gamma_2,\beta_2) = (-0.56858852, 0.70005423, -0.9593774, 0.40289732)$. The probability distributions of the final quantum states from QAOA are presented in Figs. 8(a) and 8(b). It can be observed that the ability of standard QAOA to find the optimal solution $|00110\rangle$ notably lags behind that of enhanced MQAOA. For instance, the projection probability of the optimal solution in round-2 MQAOA approaches 1, while it is approximately 0.5 in depth-2 QAOA.

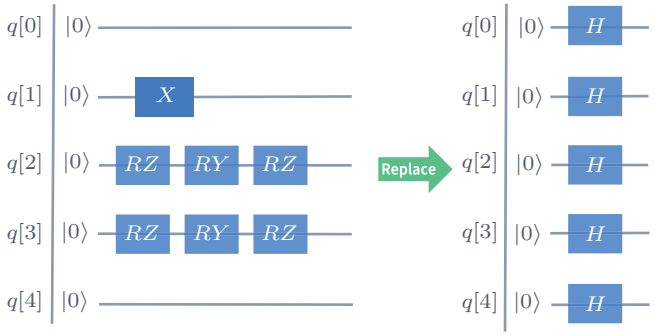


Fig. 9. Differences in the quantum circuit of round-2 MQAOA compared with round-1 MQAOA. $RZ(2,-0.105370)$, $RZ(3,0.596030)$, $RY(2,1.989450)$, $RY(3,0.448480)$, $RZ(2,0.105370)$, $RZ(3,-0.596030)$.

The results of the validation are summarized in Table 3, where the ground-state overlap represents the success probability of an algorithm finding the optimal solution as defined in Ref. [11]. The results confirm that round-1 MQAOA yields a 66.3% decrease in energy error compared with depth-1 QAOA, and a 233% increase in ground-state overlap (success probability). When MQAOA is run to the second round, the ground-state overlap (success probability) reaches approximately 0.97. This implies that MQAOA achieves considerably higher computational efficiency compared with standard QAOA.

Table 3. Performance metrics of QAOA and MQAOA for solving Max-2-SAT problem.

	Depth-1 QAOA	Depth-2 QAOA	Round-1 MQAOA	Round-2 MQAOA
Energy error	2.20057	1.48598	0.74212	0.09267
Ground state overlap	0.27457	0.48899	0.66808	0.96924

4.2. Solving Max-3-SAT Problem by enhanced MQAOA

Another instance is a Max-3-SAT problem with 5 bits and 25 clauses, whose Boolean expression is

$$\begin{aligned}\Phi = {} & (\neg x_0 \vee \neg x_1 \vee x_2) \wedge (\neg x_0 \vee x_1 \vee \neg x_2) \wedge (\neg x_0 \vee \neg x_3 \vee x_1) \\ & \wedge (\neg x_0 \vee \neg x_3 \vee \neg x_2) \wedge (\neg x_0 \vee x_3 \vee \neg x_2) \wedge (\neg x_0 \vee x_3 \vee x_4) \\ & \wedge (x_0 \vee \neg x_1 \vee \neg x_2) \wedge (x_0 \vee x_1 \vee \neg x_2) \wedge (x_0 \vee x_1 \vee \neg x_4) \\ & \wedge (x_0 \vee \neg x_3 \vee \neg x_2) \wedge (x_0 \vee \neg x_3 \vee x_2) \wedge (x_0 \vee \neg x_3 \vee x_4) \\ & \wedge (x_0 \vee x_3 \vee \neg x_1) \wedge (x_0 \vee x_3 \vee \neg x_4) \wedge (x_1 \vee x_2 \vee \neg x_4) \\ & \wedge (\neg x_3 \vee \neg x_1 \vee \neg x_2) \wedge (\neg x_3 \vee \neg x_1 \vee \neg x_4) \\ & \wedge (\neg x_3 \vee x_1 \vee x_4) \wedge (\neg x_3 \vee \neg x_2 \vee x_4)\end{aligned}$$

$$\wedge(\neg x_3 \vee x_2 \vee x_4) \wedge (x_3 \vee \neg x_1 \vee x_2)$$
$$\wedge(x_3 \vee \neg x_1 \vee x_2) \wedge (x_3 \vee \neg x_2 \vee \neg x_4)$$
$$\wedge(x_3 \vee \neg x_2 \vee x_4) \wedge (x_3 \vee x_2 \vee \neg x_4). \quad (17)$$

The weighted connection graph is illustrated in Fig. 10, and the corresponding weighted maximal matching is given by $M = [(0,1),(2,3)]$, with the sum of the weights of the matched edges attaining a maximum value of 19. The coefficients of the terms in the problem Hamiltonian are presented in Table 4, with the coefficients of the unmentioned terms being zero.

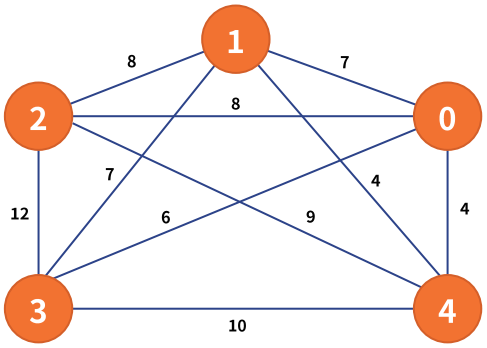


Fig. 10. The weighted connection graph for the instance of the Max-3-SAT problem.

Table 4. Coefficient for each item of the problem Hamiltonian of the Max-3-SAT problem.

h_0	h_1	h_2	h_3	f_{01}	f_{03}	f_{04}	f_{13}	f_{24}
2	−1	−5	−1	−1	−1	−2	−3	−2
f_{34}	g_{012}	g_{014}	g_{034}	g_{123}	g_{124}	g_{134}	g_{234}	
−4	2	−1	−3	−1	−1	−2	−1	

The evolution of the terms in the problem Hamiltonian can be decomposed into a combination of quantum logic gates

$$e^{-i\frac{h_i\gamma}{8}\sigma_z^i} = RZ(i, h_i\gamma/4),$$
$$e^{-i\frac{f_{ij}\gamma}{8}\sigma_z^i\otimes\sigma_z^j} = \mathrm{CNOT}(i,j)\cdot RZ(j, f_{ij}\gamma/4)\cdot \mathrm{CNOT}(i,j),$$
$$e^{-i\frac{g_{ijk}\gamma}{8}\sigma_z^i\otimes\sigma_z^j\otimes\sigma_z^k} = \mathrm{CNOT}(i,j)\cdot \mathrm{CNOT}(j,k)\cdot RZ(k, g_{ijk}\gamma/4)$$
$$\times \mathrm{CNOT}(j,k)\cdot \mathrm{CNOT}(i,j). \quad (18)$$

The quantum circuit for this instance of the Max–3–SAT problem is shown in Fig. 11.

The probability distribution of the quantum state prepared by round-1 MQAOA is depicted in Fig. 12(c), and that from round-2 MQAOA with slight changes in the quantum circuit described in Fig. 13 is shown in Fig. 12(d). The probability distributions of quantum states obtained from depth-1 QAOA and depth-2 QAOA, with time parameters for depth-2 QAOA set to $(\gamma_1, \beta_1, \gamma_2, \beta_2) = (-0.55635074, 0.51319259, -0.82876299, 0.31973179)$, are shown in Figs. 12(a) and 12(b). The performance parameters corresponding to the above cases are compared in Table 5.

The results of the validation reveal that round-1 MQAOA yields a 33% decrease in energy error compared with depth-1 QAOA, and a 210% increase in ground-state overlap (success probability). When MQAOA is run for the second round, the ground-state overlap (success probability) reaches approximately 0.78. The energy error further decreases to around 0.5, which is only one-third of the energy error of depth-2 QAOA. Overall, the performance of MQAOA significantly outperforms that of standard QAOA.

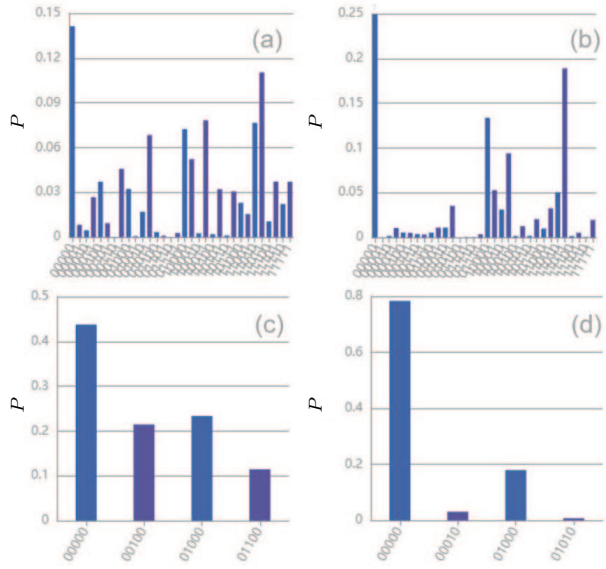


Fig. 12. The probability distributions of the quantum states from QAOA and MQAOA for solving the instance of the Max-3-SAT problem. (a) depth-1 QAOA; (b) depth-2 QAOA; (c) round-1 MQAOA; (d) round-2 MQAOA.

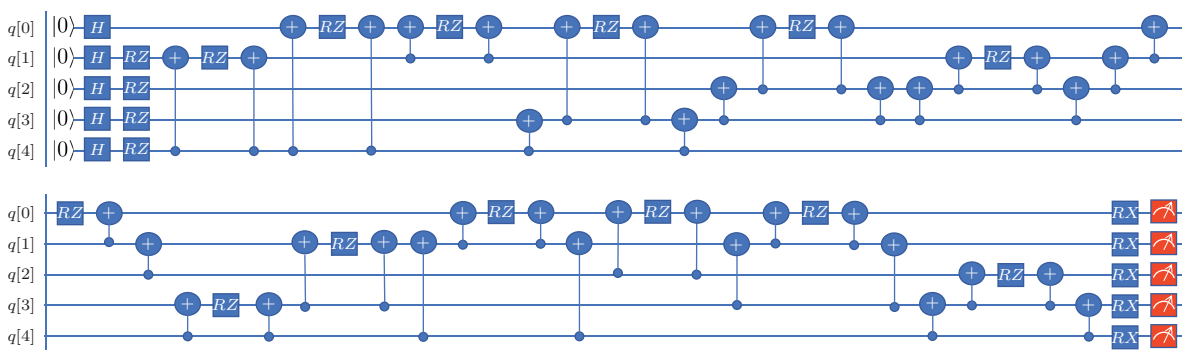


Fig. 11. The quantum circuit of depth-1 QAOA embedded in round-1 MQAOA for solving the instance of the Max-3-SAT problem. Time parameters $(\gamma, \beta) = (-0.74284694, 0.38554442)$.

Table 5. Performance metrics of QAOA and MQAOA for solving Max-3-SAT problem.

	Depth-1 QAOA	Depth-2 QAOA	Round-1 MQAOA	Round-2 MQAOA
Energy error	2.02197	1.59109	1.35349	0.50121
Ground state overlap	0.14119	0.24926	0.43824	0.78322

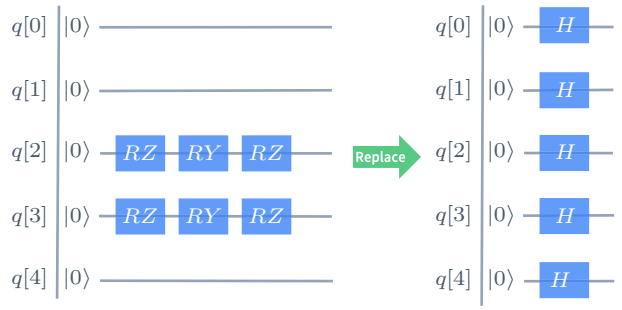


Fig. 13. Changes in quantum circuit of round-2 MQAOA. $RZ(2,-0.904320)$, $RZ(3,-0.324150)$, $RY(2,1.221320)$, $RY(3,1.261610)$, $RZ(2,0.904320)$, $RZ(3,0.324150)$.

5. Summary

In Ref. [22], the Multiscale Quantum Approximate Optimization Algorithm (MQAOA) integrates renormalization group (RG) transformations with QAOA to address the exponentially growing computational cost and reachability deficits encountered in standard QAOA. The graph inherent in the problem Hamiltonian is used to guide the partition of qubits into blocks, and all edges are treated equally in the maximal matching strategy. Based on this, RG transformations are performed on the blocks. For problem Hamiltonians including three-body and higher-order interactions, the graph structure is not always explicit. Here, we propose a method to construct a connection graph of variables directly from the problem formula and assign different weights to edges according to the frequency of occurrence of connections between the same two variables in the formula. Numerical analysis and validation on quantum simulators show that this approach enhances MQAOA's performance in solving multibody combinatorial optimization problems. The results reveal that the enhanced MQAOA can identify the optimal solution by the fourth round of optimization on average, whereas standard QAOA requires up to six layers to achieve the optimal solution. The findings regarding the impact of clause density suggest that increasing clause density does not degrade the computational accuracy of enhanced MQAOA, effectively mitigating the reachability deficits inherent in standard QAOA. The validation on the Origin quantum simulator indicates that enhanced MQAOA with depth-1 QAOA can converge to the optimal solution more efficiently than standard QAOA. This is reasonable since deeper QAOA circuits are considerably more challenging to implement than shallow ones, particularly in terms of the required number of quantum gates and gate operation times, which are major constraints for current quantum hardware.

The application of MQAOA introduces an additional operation: after obtaining the ansatz state with optimized QAOA parameters, the reduced density matrix ρ_{ij} of each block is reconstructed via quantum measurements. For an N-qubit system, there are at most $N/2$ blocks, where each block corresponds to a two-qubit subsystem. Reconstructing the density matrix of a two-qubit subsystem requires measuring 15 observables, resulting in a total of $(15N)/2$ observables. Notably, this number does not scale exponentially with the number of qubits and is significantly smaller than the number of observables required in standard QAOA. Given MQAOA's efficiency in finding solutions, compared with standard QAOA, it can achieve superior performance by incorporating only a shallow QAOA, while consuming fewer measurement resources.

The maximum matching algorithm required for graph preprocessing in MQAOA is a highly efficient classical algorithm and does not constitute a bottleneck despite the reduction in the required QAOA depth. Moreover, the method used to construct the connection graph does not affect its computational complexity. Furthermore, the QAOA component in this framework can be replaced by other variants, such as those in Refs. [14–18]. This flexibility facilitates applications on a broader scale. In practice, the connectivity between qubits in real quantum devices may vary, which in turn affects the performance of block partitioning in weighted matching. Incorporating the connectivity topology of physical qubits into the weighted matching-based partitioning—while distinguishing between interacting and non-interacting qubit pairs—is an interesting direction for future research, which we will address in subsequent work.

Acknowledgments

Project supported by the National Natural Science Foundation of China (Grant Nos. 62371199 and 62071186) and Guangdong Provincial Quantum Science Strategic Initiative (Grant Nos. GDZX2303007 and GDZX2305001).

References

[1] Bharti K, Cervera-Lierta A, Kyaw T H, Haug T, AlperinLea S, Anand A, Degroote M, Heimonen H, Kottmann J S, Menke T, Mok W K, Sim S, Kwek L C and Aspuru-Guzik A 2022 *Rev. Mod. Phys.* **94** 015004

[2] Peruzzo A, McClean J, Shadbolt P, Yung M H, Zhou X Q, Love P J, Aspuru-Guzik A and O'Brien J L 2014 *Nat. Commun.* **5** 4213

[3] Li Y and Benjamin S C 2017 *Phys. Rev. X* **7** 021050

[4] Farhi E, Goldstone J and Gutmann S 2014 arXiv:1411.4028 [quant-ph]

[5] Blekos K, Brand D, Ceschini A, Chou C, Li R, Pandya K and Summer A 2024 *Phys. Rep.* **1068** 1

[6] Papalitsas C, Andronikos T, Giannakis K, Theocharopoulou G and Fanarioti S 2019 *Algorithms* **12** 224
[7] Bourreau E, Fleury G and Lacomme P 2025 arXiv:2505.01214 [quant-ph]
[8] Ding Q M, Huang Y M and Yuan X 2024 *Phys. Rev. Applied* **21** 034036
[9] Papalitsas C, Guan Y, Waghe S, Liakos A, Balatsos I and Pantazopoulos V 2025 arXiv:2503.04239 [cs.ET]
[10] Akshay V, Philathong H, Moracles M E S and Biamonte J D 2020 *Phys. Rev. Lett.* **124** 090504
[11] Akshay V, Philathong H, Campos E, Rabinovich D, Zacharov I, Zhang X M and Biamonte J D 2022 *Phys. Rev. A* **106** 042438
[12] Campos E, Rabinovich D, Akshay V and Biamonte J 2021 *Phys. Rev. A* **104** L030401
[13] McClean J R, Boixo S, Smelyanskiy V N, Babbush R and Neven H 2018 *Nat. Commun.* **9** 4812
[14] Wang Z, Zheng P L, Wu B and Zhang Y 2023 *Phys. Rev. Res.* **5** 023171
[15] Villalba-Diez J, González-Marcos A and Ordieres-Meré J B 2021 *Sensors* **22** 244
[16] Herrman R, Lotshaw P C, Ostrowski J, Humble T S and Siopsis G 2022 *Sci. Rep.* **12** 6781
[17] Chandarana P, Hegade N N, Paul K, Albarrán-Arriagada F, Solano E, del Campo A and Chen X 2021 *Phys. Rev. Res.* **4** 013141
[18] Yu Y, Cao C, Dewey C, Wang X B, Shannon N and Joynt R 2022 *Phys. Rev. Res.* **4** 023249
[19] Lee X, Saito Y, Cai D and Asai N 2021 *IEEE International Conference on Quantum Computing and Engineering (QCE)* pp. 10
[20] Fernández-Pendás M, Combarro E F, Vallecorsa S, Ranilla J and Rúa I F 2022 *J. Comput. Appl. Math.* **404** 113388
[21] Shaydulin R, Hadfield S, Hogg T and Safro I 2021 *Quantum Inf. Process* **20** 359
[22] Zou P 2025 *Phys. Rev. A* **111** 012427
[23] Wilson K G 1975 *Rev. Mod. Phys.* **47** 773
[24] Romero S V, Visuri A M, Cadavid A G, Simen A, Solano E and Hegade N N 2025 *Commun. Phys.* **8** 348
[25] Moret B M E 1988 *SIGACT News* **19** 51